Summary of a Bearingless Motor with Passive Electrodynamic Axial Suspension

Guilherme Cavalcante Rubio[1], Yusuke Fujii[1], and Akira Chiba[1]
[1] Tokyo Institute of Technology, Meguro, Tokyo, Japan
cavalcante.g.aa@m.titech.ac.jp
fujii@ee.e.titech.ac.jp
chiba@ee.e.titech.ac.jp

1 Introduction

Either active control or passive stabilization can be used to achieve non-contact magnetic suspension in magnetic bearings and bearingless motors. As the rotational speed is increased, the *d*-axis current becomes harder to regulate, thus motivating the research of full passive suspension. Permanent magnet bearings and reluctance forces cannot stabilize all Degrees Of Freedom (DOF) by themselves, therefore, complementary passive methods are required to achieve full passive suspension in bearingless motors.

Among several passive suspension techniques, electrodynamic suspension is chosen for this machine, because the same coils that generate motor torque can be used for passive stabilization and it does not require superconductors with a dedicated cooling system.

Passive electrodynamic suspension in rotating machines has been already explored in several structures. It was applied to both passive electrodynamic bearings [1] and bearingless motors [2]–[4]. This paper reports an improvement of a previously reported bearingless motor with passive axial suspension through figure-eight coils previously presented in an IEEE IAS cosponsored conference paper [4]. It suffered from low axial force due to the low radial flux density. This electrodynamic suspension principle on axial direction is similar to previously published machines [2], [3]. In this paper, magnetic flux density and, consequently, axial electrodynamic force at low rotational speed are significantly increased when compared to the previous model [4]. A prototype machine is built to confirm the axial force characteristics.

2 Suspension Principle

Fig. 1 show a planar view of the figure-eight coil [2] A_1. The rotor has surface-mounted permanent magnets that generate a sinusoidal magnetic field. This magnetic field is represented by an array of vectors entering and leaving the coil plane. The permanent magnet rotates at a constant angular speed ω in radians per second. When the rotor is displaced from the axial center, there is an imbalance between fluxes linked by the upper and lower coils. Consequently, a suspension current i_{za1} circulates inside the figure-eight coil. Through the interaction of this current and the rotor magnetic field, stabilizing electrodynamic forces are generated in the stator coils, as indicated by blue arrows in Fig. 1.

Fig. 2 shows the equivalent electrical circuit for the figure-eight coil A_1. The upper and lower coils are assumed to have identical shape, identical number of turns n, identical resistance R, and identical self-inductance L. Defining the number of figure-eight coils in the stator c, the number of pole pairs p, and the constant K_λ, equivalent to the derivative of flux linkage in the upper and lower coils in terms of axial displacement z, the total axial electrodynamic force on the stator is derived as

$$F_{ze\,T} = \frac{c\,{K_\lambda}^2\,p^2\,\omega^2 L\,z}{(R^2 + p^2\omega^2 L^2)}. \tag{1}$$

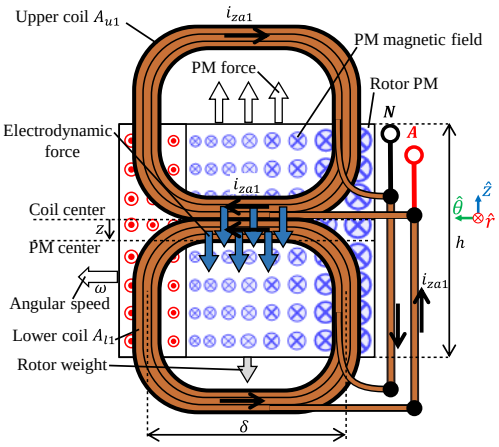

Fig. 1. Planar view of figure-eight coil A_1

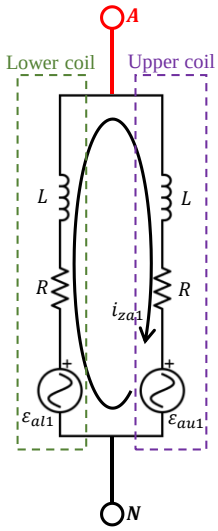

Fig. 2. Equivalent circuit of figure-eight coil A_1

3 Improvements of the Motor Structure

Figs. 4(a)-(d) show the initial structure Motor 1 [4] and the improved structures that derived from the initial machine. Motor 1 has a two-pole permanent magnet rotor and six figure-eight coils evenly distributed in the stator. To avoid unstable radial attraction forces, there are no ferromagnetic materials in the stator. The air gap flux density is very low, resulting in low axial electrodynamic force. Structural improvements were done to increase the air gap flux density and suspension force, so that the minimum rotational speed for full passive suspension is decreased.

Fig. 4(b) shows the structure of Motor 2. To increase radial flux density, two rotating back-iron were attached to the shaft. The outer and inner rotating parts are mechanically connected by an aluminum frame. The stationary coils are now surrounded by rotating parts. The leakage flux is reduced and a path with high magnetic permeability is created. Because there are no ferromagnetic parts in the stator, unstable attraction force is not generated. The number of poles was changed from two to four, so electrical frequency was doubled. The PM material was changed from neodymium N40 to N50.

Fig. 4(c) shows the improved structure Motor 3. Two permanent magnet rings are added to the rotor of Motor 2. One is on the upper side and another is on the lower side. Both have polarization opposite to that of the original central permanent magnet. Flux-linkage variation with displacement z becomes twice that of Motor 2. Owing to the increased ratio of magnetic flux linkage variation over displacement and to the force generated in the upper and lower coils ends, it is found that the electrodynamic force in Motor 3 is approximately four times higher than that of Motor 2.

Fig. 4(d) shows the final improved structure Motor 4. The radial component of the magnetic flux density, and, consequently, the magnetic flux linkage are increased by attaching additional permanent magnets to the outer shell. The magnetization direction is aligned with the PM on the inner rotor. The total volume of permanent magnets attached to the rotor is increased. Not only the peak radial flux density is increased, but it is also more uniform along the air gap between both permanent magnet surfaces than what is observed in Motor 3.

Fig. 5 shows a comparison of axial electrodynamic forces for $z = 1$ mm. These forces are calculated through 3D FEA among Motors 1, 2, 3, and 4 for rotational speeds up to 50 krpm. The axial force increases as the rotational speed is increased. At 45 krpm, Motor 4 achieved an axial force approximately 77 times higher than that of the initial structure, Motor 1.

To validate the equation for total axial electrodynamic force, the experimental value of K_λ is substituted in (1). The results of equation (1) for $z = -0.49$ mm are compared to both the FEA and experimental results for a range of rotational speeds up to 2400 rpm in steps of 300 rpm. The

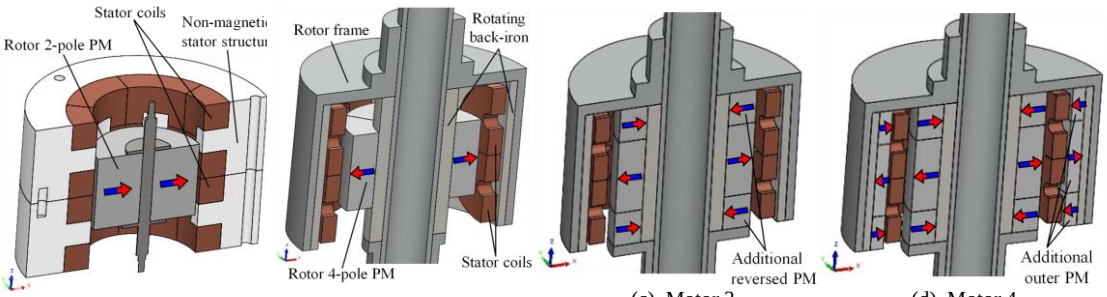

(a) Motor 1 (b) Motor 2 (c) Motor 3 (d) Motor 4

Fig. 4. Improvements upon the initial structure Motor 1. Each improved motor has higher axial electrodynamic stiffness than the previous one.

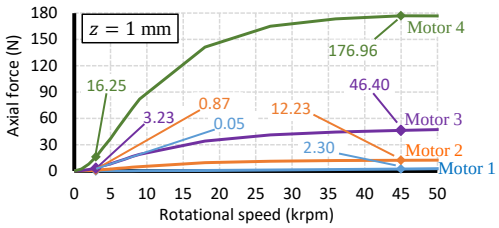

Fig. 5. Improved axial force calculated through FEA

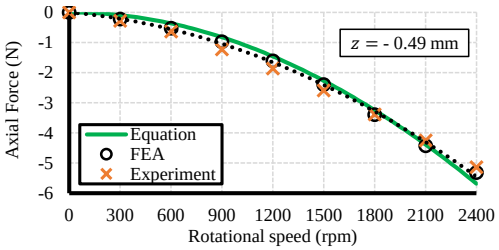

Fig. 6. Experimental axial force measured for Motor 4

axial force increases with rotational speed. At 2400 rpm, FEA and measured force were -5.31 N and -5.14 N, respectively. Discrepancy is -3.2%. The divergence observed between the equation, FEA and experimental values occurs due to uncertainties in K_λ, self-inductance, and resistance. The resistance value is dominant in this range of rotational speeds, since the coil inductive reactance is about 20% of the resistance at 2400 rpm. The constant K_λ affects force at all rotational speeds.

4 Conclusion

This paper shows the structure improvement of a bearingless motor with electrodynamic suspension in the axial direction. The motor was improved in three steps from the initial structure. The electrodynamic axial force of Motor 4 measured through the experiment was about 180 times higher than the one calculated for Motor 1 through FEA at 2400 rpm. A prototype was built for Motor 4, the machine with highest axial stiffness. The electrodynamic axial stiffness was measured for a range of rotational speeds and fixed axial displacement z.

References

[1] J. Sandtner and H. Bleuler, "Electrodynamic passive magnetic bearing with planar halbach arrays," in *Proceedings of the 9th international symposium on magnetic bearings*, 2004, pp. 3–6.

[2] H. Matsue, "Electromagnetic property of bearingless motor based on electro-magnetic induction," *Railway Technical Research Institute Report*, vol. 25, no. 3, pp. 47–52, 2011.

[3] J. Van Verdeghem and B. Dehez, "Fully Passively Levitated Self-Bearing Machines with Combined Windings," in *2020 IEEE Energy Conversion Congress and Exposition (ECCE)*, Oct. 2020, pp. 254–261, doi: 10.1109/ECCE44975.2020.9235412.

[4] G. Cavalcante Rubio and A. Chiba, "Design and analysis of a bearingless motor with passive axial suspension through null-flux coils," in *2019 IEEE International Electric Machines and Drives Conference, IEMDC 2019*, 2019, pp. 779–786, doi: 10.1109/IEMDC.2019.8785077.